Classifying compound coastal storm and heavy rainfall events in the north-western Spanish Mediterranean

Marc Sanuy[1], Tomeu Rigo[2], José A. Jiménez[1], M. Carmen Llasat[3]

[1]Laboratori d'Enginyeria Marítima, Universitat Politècnica de Catalunya, BarcelonaTech, c/Jordi Girona 1-3, Campus Nord ed. D1, Barcelona, 08034, Spain
[2]Servei Meteorològic de Catalunya, C. Berlin, 38-46, 08029, Barcelona, Spain
10 [3]GAMA, Department of Applied Physics, University of Barcelona, Barcelona, 08028, Spain

Correspondence to: Marc Sanuy (marc.sanuy@upc.edu)

Abstract. The Northwest (NW) Mediterranean coastal zone is a populous and well-developed area in which the impact of natural hazards like flash floods and coastal storms can result in frequent and significant damages. Although the occurrence and impacts of such hazards have been widely covered, few studies have considered their combined impact on the region, which would result in more damage. Within this context, this study analyses the occurrence and characteristics of compound

15 extreme events of heavy rainfall episodes (as a proxy for flash floods) and coastal storms (using the maximum significant wave height) along the Catalan coast as a paradigm of the NW Mediterranean. Two different types of events are considered: multivariate, in which the two hazards occur at the same location, and spatially compounding, in which they occur within the same limited time window and their impacts accumulate at distinct and separate locations. The analysis is regionally performed

20 along a coastline extension of about 600 km by considering seven coastal sectors and their corresponding river catchment basins. Once the compound events are analysed, the synoptic atmospheric pressure fields are analysed to determine the prevailing weather conditions that generated them. Finally, a Bayesian network is used to fully characterise these events over the territory. The obtained results show that the NW Mediterranean, represented by the Catalan coast, has a high probability of experiencing compound extreme events (3.4 events per year). Despite the relatively small size of the study area (600 km of

25 coastline), there are significant variations in the event characteristics along the territory, with the most frequent type being spatially compound, except in the northernmost sectors where multivariate events dominate. These northern sectors also present the highest correlation in the intensity of both hazards. Three representative synoptic situations have been identified as dominant for the occurrence of these events, with different relative importance levels of the compounding drivers (rainfall and waves) and different distributions of impacts across coastal basins. Overall, the results indicate that heavy rainfall has the more

30 significant damage impact despite the wave damage having a larger spatial reach.

1. Introduction

Coastal zones are one of the highest risk areas in the world given the concentration of natural hazards, people, and buildings along coastlines (e.g. Kron, 2013). Among the different hazards, flooding is currently the most frequent, dangerous, and costly (IPCC, 2012; Blöschl et al., 2020), and it is very likely to significantly increase under climate change (e.g. Hallegatte, 2013;

35 IPCC, 2014; Alfieri, 2015; Blöschl, 2017). One of the intrinsic characteristics of flooding in coastal areas is that it can be induced by different climatic drivers such as storm surge, run-up, rainfall, and/or river flow, each of which may act individually but are often interconnected (Berghuijs, 2019). Moreover, when flooding is induced by marine drivers, such as storm surge and waves, impacting sedimentary coastlines, erosion also occurs simultaneously. Thus, although risk assessments in coastal zones usually consider the impact of sea hazards and climate drivers individually (e.g. Michaelides et al., 2018; Van Dongeren

40 et al., 2018), they should instead be considered as the result of compounding events (Hao et al., 2018; Ward et al., 2018). In this sense, an increasing number of studies have stressed the importance of compound flooding in coastal zones at different

geographical scales (Wahl et al., 2015; Paprotny at al., 2018; Wu et al., 2018; Bevacqua et al., 2019; Hendry et al., 2019), including their potential increase under the influence of climate change (Moftakhari et al., 2017; Bevacqua et al., 2019). When the importance of these types of events is considered across Europe, the Mediterranean coastline can be considered a hotspot.

45 On the one hand, more than 50% of its population is concentrated in the coastal zone, increasing the risk to human life due to flooding (Vinet et al., 2019). On the other hand, the relative frequency of flash floods in the region is the highest in Europe (Gaume et al., 2016), and impacts related to climate and environmental changes are more severe relative to the global average, with temperatures already reaching +1.5 °C relative to pre-industrial times (Cramer et al., 2018). This combination also implies an increase in coastal storm–induced damage over the last few decades (e.g. Jiménez et al., 2012; Garnier et al. 2018). However,

50 there are a limited number of studies assessing the combined effect of different hazard-inducing climate drivers (Hall et al., 2014). In the Northwest (NW) Mediterranean, Ballesteros et al. (2018) analysed and compared the risk of flooding in the central part of the Catalan coast due to flash floods, storm waves, and sea-level rise; they concluded that flash floods induce higher risks in comparison with marine-related flooding, even though they are acting on a smaller spatial scale along the coastline. However, they did not consider these different drivers to jointly contribute to compound flooding. With respect to

55 compound flooding, most of the existing analyses are part of very large-scale studies (Paprotny et al., 2018; Bevacqua et al., 2019), with few examples at local scales (Wahl et al., 2015; Wu et al., 2018; Hendry et al., 2019). Among them, Bevacqua et al. (2019) identified Mediterranean coasts as the European areas with the highest probability of compound flooding under present conditions. As is the case with most existing studies of compound flooding, they inferred that storm surge and precipitation were climate drivers that would act simultaneously. When characterising coastal compound flooding from a risk-

60 oriented perspective, the definition of the compound event itself and the choice of contributing climatic drivers are key aspects to be considered. Recently, Zscheischler et al. (2020) proposed a classification of compound events into four main types, which facilitates the analysis of the mechanisms driving the impact and thereby provides a framework for risk adaptation. Using these classifications, this study considers and analyses two main types of events: multivariate and spatially compounding.

65 A *multivariate compounding event* refers to the co-occurrence of hazards from multiple climate drivers in the same geographical region. This is the most common type of event when analysing compound coastal flooding, as defined by the co-occurrence of a marine driver (usually storm surge) and a 'terrestrial' one such as rainfall or river flow acting at the same site (e.g. Wahl et al., 2015; Hendry et al., 2019). Due to the characteristics of coastal storms in the NW Mediterranean, waves are considered the main marine driver controlling the floodwater volume to the hinterland, since the wave-induced run-up, Ru, is

70 much larger than the magnitude of the storm surge (e.g. Mendoza and Jiménez, 2009; Mendoza et al., 2011). Moreover, the use of storm waves as the marine driver also potentially indicates the importance of interconnected erosion hazards (in addition to flooding). On the other hand, due to the nature of flooding in the NW Mediterranean coastal zone, heavy rainfall episodes are considered the main terrestrial drivers (as a proxy for runoff), which lead to flash floods (Cortès et al., 2018; Gaume et al., 2019).

75

Spatially compounding events refer to co-occurring hazards from different climate drivers within a limited time window, accumulating impacts at spatially distant locations. From a risk management standpoint, these events are very relevant because they may overwhelm the capability of emergency-response services since these have to respond to a large number of emergency situations throughout the region at the same time. In this study, these events are defined by the co-occurrence of

80 the two above-mentioned hazards, heavy rainfall and coastal storms, within a time window of three days along the Catalan coast (NW Mediterranean, Spain). Thus, a location under such an event will experience only heavy rainfall or a coastal storm that will accumulate with hazards happening simultaneously, or in rapid succession, in other parts of the territory.

To put this study in the context of risk management, this work will also illustrate the associated impact of selected compound

85 events. In any case, the impact is likely the result of a combination of climatic and societal drivers, with the climate drivers controlling the magnitude of the hazards (analysed herein) and the societal drivers causing an increase or decrease in the associated impacts (e.g. Raymond et al., 2020). One of the problems in properly accounting for these impacts in large geographical areas is the difficulty in obtaining after-event local data across the entire territory. However, a way to identify remarkable events is by considering the significance of their associated impacts in qualitative terms by analysing after-event

90 press coverage and/or insurance data. In the study area, this has been done previously by Llasat et al. (2009) and Cortès et al. (2018) for flash floods and by Jiménez et al. (2012) for coastal storms. This will also be the approach adopted to illustrate the impact of selected events herein.

Within this context, the main aim of this work is to characterise the occurrence of compound flooding events along the Catalan

95 coast (representative of the NW Mediterranean). To this end, we investigated the dependency between coastal storms and intense rainfall for the two types of compound events previously introduced: multivariate events, in which we search for the simultaneous presence (within a time range of three days) of a coastal storm and a heavy rainfall episode in the same geographical area, and spatially compounding events, in which we search for the simultaneous presence (within a time range of three days) of a coastal storm and a heavy rainfall episode in different geographical areas. Thus, (i) we quantify the

100 occurrence frequency of the different types of compound events; (ii) we analyse the spatial variability of the different types of compound hazards and the dependence between extreme variables (rainfall and wave height); and (iii) we examine the prevailing synoptic meteorological patterns during the compound events to identify whether the meteorological drivers can be distinguished in terms of event type (multivariate vs. spatially compounding) and the intensity of the drivers. Finally, some examples of the identified events are outlined in terms of their characteristics and induced impacts.

105

The remainder of this paper is organised as follows. Section 2 introduces the study area and describes the data used. Section 3 presents the methodology used in the analysis. Section 4 presents the results of analysing compound events along the Catalan coast. Section 5 discusses these results and illustrates the different types of compound events with selected remarkable events occurring in the study area during the last 30 years. Finally, conclusions are presented in Section 6.

110 **2. Study area and data**

2.1. Study area

The study domain is located in the north-east of the Iberian Peninsula and consists of the coastal zone along Catalonia and the river basins flowing into it, which are composed of the internal river basins of Catalonia and the Ebro lower river basin (Figure 1). The coastline runs in the SE–NE direction and is bounded by the presence of two parallel mountain ranges located close to

115 the sea: the littoral range (maximum altitude around 600 metres above sea level, masl) and the pre-littoral range (maximum altitude around 1800 masl). The northern part of the region is limited by the Pyrenees, running from west to east, with altitudes greater than 2000 masl. Therefore, the region is prone to the development of flash floods and thunderstorms (Llasat et al., 2014b), both from a hydrological point of view (existence of many small torrential catchments) and from a meteorological point of view (i.e. orographic forcing of Mediterranean air masses) (Llasat and Puigcerver, 1992). In fact, the impact of

120 mountains on the low-level wind circulation usually triggers convective instability and affects the pressure fields (Jansà et al., 2014).

The Catalan coastline extends about 600 km, of which ~280 km corresponds to sedimentary coasts. The combination of the decrease in river sediment supplies, current level of urbanisation and infrastructure development, and the natural littoral

125 dynamics has led to an overall shoreline erosion during the last few decades (Jiménez and Valdemoro, 2019). From the perspective of coastal storms, the area is subjected to dominant NE–E extreme waves as well as secondary impacts from the S–SE (Mendoza and Jiménez, 2009; Bolaños et al., 2009; Mendoza et al., 2011). The NW Mediterranean is a microtidal environment with an astronomical tidal range of about 0.25 m. Meteorological tides are of low amplitude, reaching maximum recorded values up to 0.5 m during favourable conditions (under low atmospheric pressure centres and landward-blowing

130 winds), in such a way that they are much lower than the wave-induced Ru during coastal storms (Mendoza and Jiménez, 2009). The order of magnitude of the storm-induced coastal hazards in the study area can be seen in Mendoza and Jiménez (2009) and Bosom and Jiménez (2011). Although the coastal storm intensity has not significantly changed (e.g. Casas-Prat and Sierra, 2010), the wave action on a progressively narrowing coastline has resulted in a significant increase in coastal damages during the last few decades (Jiménez et al., 2012).

135

To perform an integrated study of the 'terrestrial' (rainfall) and 'coastal' (waves) compound events, the study region was divided into seven areas following previous studies on flash floods (e.g. Llasat et al., 2016), dividing the region into its main groups of natural catchments along the coast (Figure 1). Each area is composed of a number of river catchments and/or groups of torrential catchments flowing to their corresponding coastal stretch.

140 **2.2. Data**

Three main climatic datasets were used in this work to characterise the rainfall, coastal storms, and weather conditions. Rainfall was characterised using daily rainfall (P24h) data obtained from the Spanish Meteorological Agency (AEMET) database (Ramis et al., 2013), which includes records from 491 automatic weather stations (AWS) in Catalonia (Figure 2) covering (non-homogeneously) the period 1950–2015. The selection criteria for identifying records to be used in this analysis consisted

145 of identifying those AWS belonging to catchments in coastal regions with a homogeneous coverage of the 41-year period from 1973 to 2013, resulting in 69 case-study rain gauges (Figure 2 and Table 1). Flood impacts were obtained from the INUNGAMA database, which contains all the flood events that have affected Catalonia since 1981 as well as all the catastrophic events since 1900 (Barnolas and Llasat, 2007; Llasat et al., 2016).

150 The wave data used were obtained from the hindcast Downscaled Ocean Waves (DOW) dataset (Camus et al., 2013), which was derived from the Global Ocean Waves dataset (Reguero et al., 2012). Data consisted of hourly values of hindcast wave conditions characterised by the significant wave height, Hs, wave period, and mean wave direction covering the same period as the rainfall data (1973–2013). The datasets were retrieved for 19 nodes located nearshore (about 20 m water depth), homogeneously covering the analysed basins along the coast (Figure 1 and Table 1) to properly capture regional variations in

155 the storm climates. Additionally, wave records during the Gloria storm in January 2020 were obtained from the SIMAR database from Puertos del Estado (www.puertos.es/es-es/oceanografia).

Weather conditions were characterised by mean sea-level pressure (MSLP) and geopotential fields at 1000 hPa from the US National Center for Environmental Protection (NCEP) datasets. NCEP/NCAR Reanalysis I (1948–present) and NCEP/DOE

160 Reanalysis II (1979–present) generated by the National Oceanic and Atmospheric Administration (NOAA) were used. In the first case, NCEP considered the same climate model that was initialised with different types of weather sources (Kalnay et al., 1996). The second version of the first reanalysis considers the starting point of the major satellite era, which implies that more observations included fewer errors in the resulting fields (Kanamitsu et al., 2002). To retrieve weather data from the NCEP/NCAR Reanalysis datasets, we used the RNCEP library of R-Cran (Kemp et al., 2012). The fields were collected for a

165 spatial extent covering longitudes −25° to 29° and latitudes 30° to 64°, with a spatial resolution of 2.5° × 2.5° (*N =13 x 15* grid) covering the period 1973–2013 with a temporal resolution of 6 h.
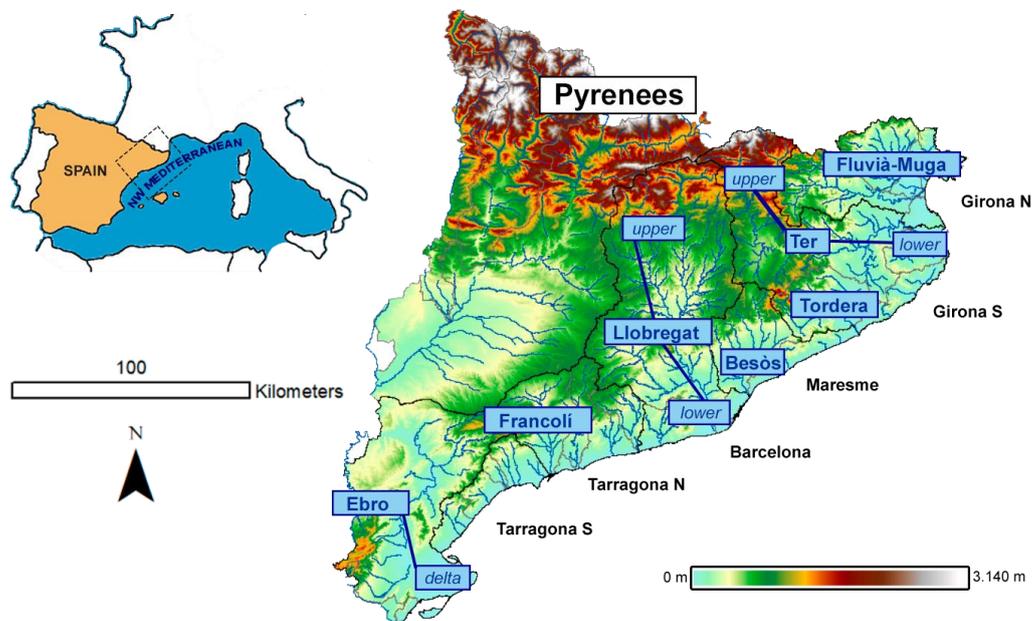
Figure 1. Study area and main coastal river systems. Digital elevation model 15x15m by Institut Cartogràfic and Geològic de Catalunya (ICGC)

170

Table 1. Number of selected rain gauges and waves nodes in the different areas along the coast (Figure 1).

ID	Basin	Rain gauges	Wave nodes
Area 1	Girona N	6	3
Area 2.a	Lower Ter and Tordera	9	3
Area 2.b	Upper Ter Basin	9	-
Area 3	Maresme	7	3
Area 4.a	Lower Llobregat basin	5	3
Area 4.b	Upper Llobregat Basin	6	-
Area 5	Tarragona N	8	2
Area 6	Tarragona S	5	2
Area 7	Lower Ebro and delta	14	3
TOTAL		**69**	**19**
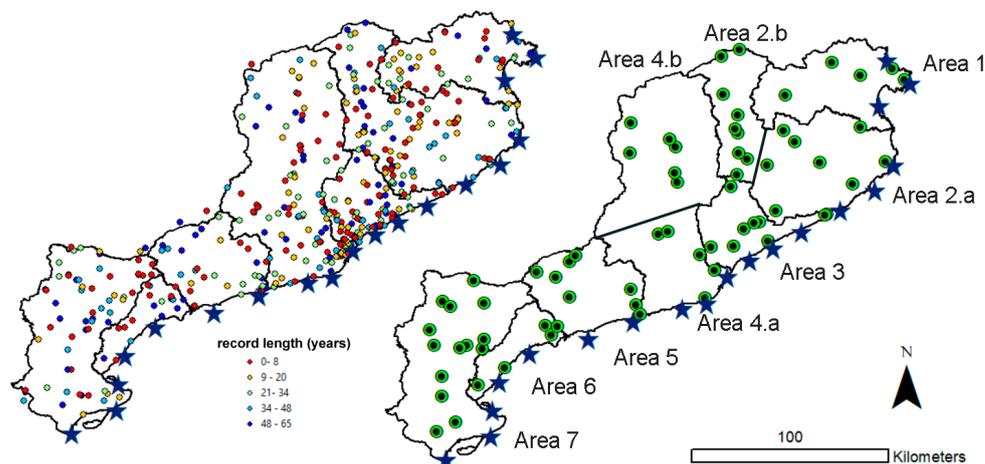
175 **Figure 2. Location of existing rain gauges, AWS (coloured dots), and wave nodes (stars) in the different drainage basins along the Catalan coast (left). Selected AWS per drainage basin (areas) along the coast (right).**

3. Methods

3.1. General framework

180 The general methodological framework adopted in this study consisted of the following steps (Figure 3):

(i) Identification of compound events. First, individual heavy rainfall and coastal storm episodes are identified at all rain gauges and coastal nodes. Then, compound events are defined by identifying dates upon which the two considered drivers verify along the territory. Extreme events with only 'pure' coastal storms without rain or 185 'pure' rain episodes without waves are discarded. Each compound event is characterised in terms of a representative Hs (the maximum value reached during the event) and daily precipitation (P24h) per coastal basin.

(ii) The results from (i) are used to assess the frequency of occurrence and spatial distribution of the different event types (multivariate and spatially compounding). At this stage, the correlation between driver intensity (i.e. the correlation between the maximum Hs and P24h) is also analysed.

190 (iii) Compound event dates obtained in (i) are used to retrieve MSLP and 1000 hPa geopotential maps, which are then classified using correlation-based techniques to determine the main associated weather types. Notably, an event can be associated with different weather types throughout its lifetime.

(iv) The results in (i) and (iii) are combined by feeding a Bayesian network (BN) to characterise each weather type in terms of the spatial distribution of the multivariate and spatially compounding events and the probabilities of 195 exceedance of driver intensities (P24h and Hs).
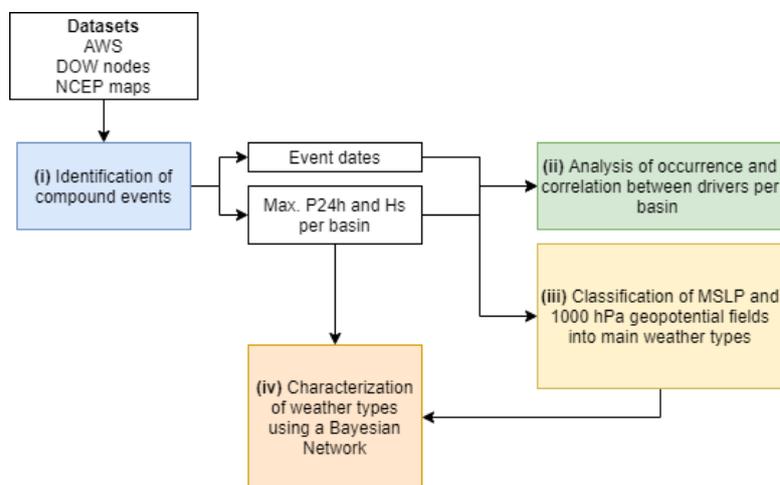
Figure 3. General methodological framework.

3.2. Identification of extreme events

200 The first step consisted of identifying individual extreme events from selected rain and wave datasets (Figure 1). This was done by applying the peak over threshold (POT) method to daily rainfall (P24h, in mm) and to significant wave height as representative climate variables of the compounding drivers: heavy rainfall and coastal storms.

Following previous studies in the area (Barbería et al., 2014; Cortès et al., 2018), potential extreme rainfall episodes were

205 identified using a P24h of 40 mm and a three-day interval between consecutive events to identify independent episodes. Although the daily threshold is below the value used by some international projects such as MEDEX (Jansà et al., 2014 proposed 60 mm), local flash floods and urban floods can be produced when this precipitation falls within less than 2 h. The event is then characterised by the maximum recorded P24h value. A second threshold of 100 mm was used to flag severe extreme events to later differentiate them during the characterisation assessments. This threshold has previously been used in

210 the region when studying extreme rainfall associated with large riverine flooding (Gilabert and Llasat, 2017).

Coastal storms were identified using a double-threshold POT (see Sanuy et al., 2019). The 98th percentile of the Hs time series is used as the first filter to locate storm start and end times, which roughly correspond to Hs = 2 m, in agreement with Mendoza et al. (2011) for NW Mediterranean conditions. Then, an upper threshold given by the 99.5th percentile is applied to retain only

215 significant storms. This criterion results in class III storms according to the Mendoza et al. (2011) classification, which corresponds to the minimum required conditions to produce significant impacts on the coast (i.e. erosion and inundation). In addition, a three-day interval of fair-weather conditions between consecutive events was used to identify independent episodes.

The result of this step is a collection of heavy rainfall and wave storm individual episodes for all AWS and wave nodes. Each

220 episode is characterised by an initial and final date and the maximum values of P24h and Hs for rainfall and waves, respectively.

3.3. Compound event classification and occurrence

The second step consisted of identifying and characterising compound events in each area along the coast (Figure 2). First, we established the occurrence of a coastal (wave) storm event by comparing the storm initial time at all coastal nodes within a 24-

225 hour window. All storms within such a window were considered a single event, which is labelled with the same date, and they

should correspond to a coastal storm propagating along the territory. Then, all rain gauges were surveyed to identify the occurrence of heavy rainfall episodes during the identified coastal (wave) storm and in the three days before. If no rainfall is registered at any rain gauge, the event is removed from the analysis, as it would correspond to a pure wave storm. On the contrary, if any station registers an extreme P24h episode, the event is flagged as a compound event, with its date of occurrence

230   being given by the earliest starting time of coastal storms at any node. Finally, each compound event is characterised by the maximum P24h and Hs values of all stations and nodes within each coastal area during the event duration.

As a result of this process, a compound event is identified herein when a heavy rainfall episode at any station along the coast occurs simultaneously, or in rapid succession (within a three-day interval), with extreme waves at any location along the coast.

235   Therefore, an identified compound event at a given time may present different spatial characteristics along the coast: areas in which rainfall and wave extreme events simultaneously verify, areas with only one extreme component (either rain or waves), and areas without any extreme episodes. Then, each compound event is characterised along the coast (in each sector) as follows: (i) multivariate (simultaneous rainfall and wave episodes); (ii) spatially compounding (SC) rain, where local extreme conditions correspond to rainfall; and (iii) spatially compounding (SC) waves, where local extreme conditions correspond to

240   storm waves.

3.4. Intensity correlation analysis

To investigate the correlation between the magnitude of both components of the compound event, P24h and Hs, across all areas, we used the Spearman rho coefficient (e.g. Genest and Favre, 2007); this is defined as the Pearson correlation coefficient between the variable ranks (eq. 1). The correlation of the wave magnitude (Hs) at each coastal area with the P24h rainfall at

245   each of the nine areas is calculated as follows:

$$\rho = \frac{cov(rg_{Hs}, rg_{P24h})}{\sigma_{rg_{Hs}}\sigma_{rg_{P24h}}} \tag{1}$$

where rg_{Hs} and rg_{P24h} are the ranks of Hs and P24h, respectively, cov is the covariance, and σ is the standard deviation.

3.5. Synoptic typology

During the development of a compound event, different weather types can be present; in this study, we therefore use

250   corresponding pressure fields (geopotential height at 1000 hPa and MSLP) at the closest time to the date-time assigned to each event (Section 3.3). Weather conditions were then classified by applying a correlation-based, gridded map-typing technique (Yarnal, 1993; Wu et al., 2018) to the 1000 hPa geopotential height field, while the MSLP maps were used in the posterior analysis of specific cases. All maps were extracted at the closest time to the beginning of the compound event, as defined in Section 3.4 (i.e. the beginning of the coastal storm). The events were grouped based on the Pearson product-momentum

255   correlation (r_{xy}, eq. 2), which depicts the degree of similarity of spatial structures between pairs of gridded data (i.e. the positions of high- and low-pressure centres, rather than their magnitudes).

First, all maps are normalised via $Zi = (zi - \bar{z})/\sigma_z$, where Zi represents the number of positive or negative standard deviations from the mean at each grid cell i, z_i is the original value at grid point i, and $\bar{z}$ and σ_z are the mean and standard

260   deviation of the $N = 13 \times 15$ grid point values. Once normalised, each map is compared with all other maps using:

$$r_{xy} = \frac{\sum_{i=1}^{N}[(x_i - \bar{x})(y_i - \bar{y})]}{\sqrt{\sum_{i=1}^{N}(x_i - \bar{x})^2(y_i - \bar{y})^2}} \tag{2}$$

where x_i and y_i represent the normalised value at each of the N points of the pair of maps being compared, and $\bar{x}$ and $\bar{y}$ are the corresponding means across the N-point grids. A pair of maps is considered similar when $r_{xy} \geq rt$, where rt is a correlation

threshold. Different sources of subjectivity exist in choosing the value of rt (Yarnal et al., 1993), which usually depends on a

265   balance between the number of identified patterns and the number of dates remaining without classification.

The process was applied as described by Wu et al. (2018). The first date of the reference is used as the key day, and all maps are compared to create the first class. Then, all classified dates are removed, and another date from the non-classified pool is used as the second key day. A value of $rt = 0.2$ was used in this step, which led to four weather-type candidates. Then, a second

270   comparison between each individual map and the average of each group candidate was performed to ensure that maps that are similar to more than one type are classified into the group corresponding to a maximum r_{xy}. This led to a final three-group classification with a mean r_{xy} of 0.64–0.7 per group.

3.6. BN-based classification

BNs are statistical tools based on acyclic graph theory and Bayes theorem (Pearl, 1988; Jensen, 1996) and have demonstrated

275   their versatility and utility in efficiently combining multiple variables to predict or characterise system behaviour (e.g. Gutierrez et al., 2011; Plant et al., 2016; Beuzen et al., 2018). The BN is used here to assess the probabilistic relationship between each type of meteorological forcing (Section 3.5) and their associated effects (multivariate or spatially compounding) and driver intensities (Hs and P24h) at each of the different basins.

280   Figure 4 shows the BN structure, the considered variables, and the variable discretisation. The arrows depict the parent–child relationships, i.e. the results will be presented in terms of the probability of given values of Hs, P24h, and impact type conditioned to the different possible combinations of the synoptic case and area. The training dataset consisted of 1260 variable combinations resulting from the previous assessment of 140 compound events in nine different areas.
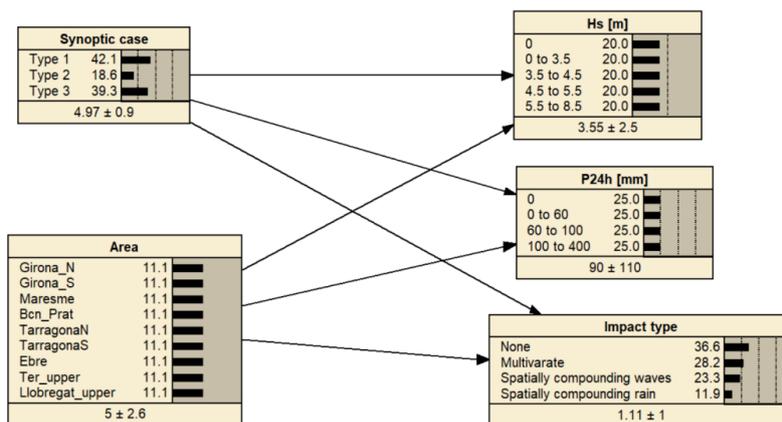
285

Figure 4. BN configuration used to characterise the system behaviour. The severity of the compounding forcing (Hs and P24h) and the presence of multivariate or spatially compounding (wave or rain only) effects are conditioned to the synoptic case (weather type) and area (basin/coastal sector).

4. Results

290   **4.1. Frequency and location of compound events**

During the analysed 1973–2013 period, 225 coastal storms and 605 heavy rainfall episodes affecting at least one of the considered areas were identified. A higher number of rainfall events was expected, since convective localised episodes should

be included based on this approach. From this total, 140 episodes can be classified as compound events in which wave storms are accompanied by the presence of heavy rainfall in any area along the coast. This means that 62% of coastal storms and 23%

295 of heavy rainfall episodes can be labelled as compound events and that the probability of having such compounding conditions is larger under coastal (wave) storms. The average frequency of occurrence along the Catalan coast during the study period was 3.4 compound events per year, without any statistically significant trend during the analysed 41 years (Figure 5).

Figure 6 and Table 2 show the spatial distribution of the 140 identified compound events along the Catalan coast according to

300 their typology as locally recorded: multivariate (simultaneous rainfall and wave storm episodes in the same area), SC-waves (a solo wave storm episode in a given area with simultaneous heavy rainfall verifying at a different location), and SC-rain (a solo rainfall episode in a given area with a simultaneous wave storm verifying at a different location). In addition, the local absence of extreme conditions for both drivers was retained.

305 The results show that, in the presence of a compound event along the Catalan coast, areas with the highest probability of experiencing a multivariate event are located in the northernmost part, Girona N, and the Lower Ter–Tordera basins (with an occurrence frequency of about 55%) followed by the southernmost end in the lower Ebro basin and delta (with an occurrence frequency of about 40%). On the other hand, although the areas located at the central part of the coast show a non-negligible probability (about 20–30% of recorded events) of experiencing multivariate events, they are dominated by the presence of

310 spatially compound events with the local presence of wave storms (about 40–50% of recorded events). These results would indicate that, in the study area, when a regional compound event occurs, wave storms are the 'spatially dominant' driver, with all areas along the coast having a probability greater than 60% of having local wave storms (either multivariate or SC-waves). On the other hand, areas presenting a high probability (>60%) of having rainfall extremes (either multivariate or SC-rain) during regional compound events are restricted to the two northernmost areas and the southernmost one (58%); the central part

315 of the coast (Areas 3 to 6) presents relatively low probabilities of experiencing extreme rainfall (35–42%).
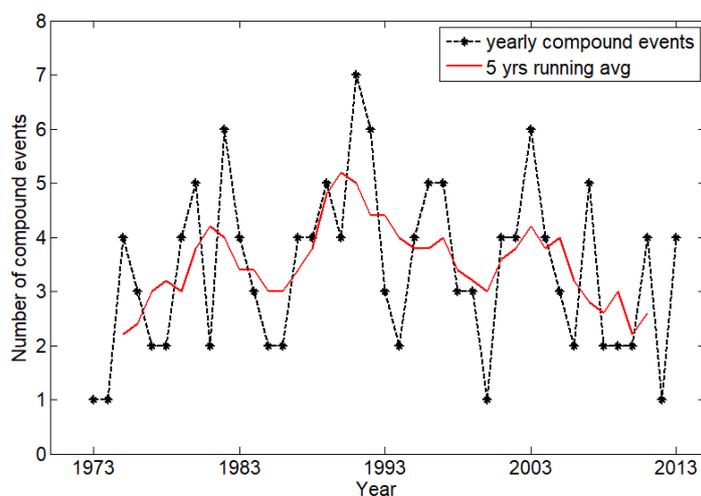
Figure 5. Annual number of compound events (black) and the running five-year average (red) for the period 1973–2013.

320 Rainfall events in the 'terrestrial' areas which correspond to the Ter and Llobregat upper basins are filtered with P24h >100 mm to assess their potential effects at the coastal fringe; fewer than 5% of cases reach those precipitation levels in combination with extreme waves at the coast.
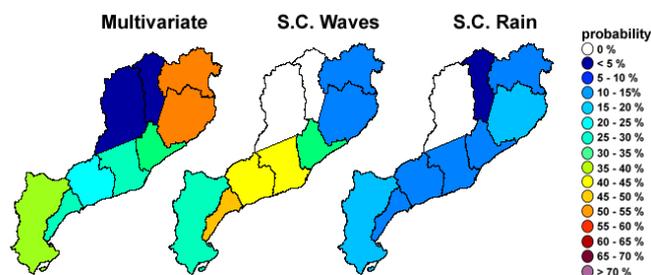
Figure 6. Probability of occurrence of the different types of compound events along the Catalan coast. Multivariate (local simultaneous rainfall and wave storm episodes); SC-waves (local wave storm episodes and simultaneous rainfall in a different area); SC-rain (local rainfall episode and simultaneous wave storm in a different area). Probabilities are given with respect to the presence of a compound event (average probability during the period 1973–2013 of about 3.4 events per year). Probabilities are given per each area along the coast, and the sum of the different types of events per area does not necessarily reach 100% due to cases in which neither rainfall nor wave storms locally verify.

Table 2. The number of compound events per type of occurrence of climatic drivers at each basin. Note that the upper basins (not directly affected by waves) are marked as (*) since the threshold of P24h > 100 mm is imposed there.

ID (Figure 1)	Basin	Multivariate	SC-waves	SC-Rain	No driver
Area 1	Girona N	70	16	19	35
Area 2.a	Lower Ter and Tordera	76	14	28	22
Area 2.b	Upper Ter Basin	3(*)	-	5(*)	132 (*)
Area 3	Maresme	43	48	17	32
Area 4.a	Lower Llobregat basin	36	58	18	28
Area 4.b	Upper Llobregat Basin	4 (*)	-	0 (*)	136 (*)
Area 5	Tarragona N	34	57	20	29
Area 6	Tarragona S	35	65	15	25
Area 7	Lower Ebro and delta	54	36	28	22

4.2. The correlation between wave components and rainfall intensity during compound events

After the probability of compound event occurrence was analysed at different areas along the coast, the correlations among the magnitude of the climatic drivers (rainfall and waves) needed to be determined. Figure 7 shows the obtained Spearman rho coefficient by correlating the waves (Hs) in each area (marked with a diamond in the figure) with rainfall (P24) at all areas along the coast.
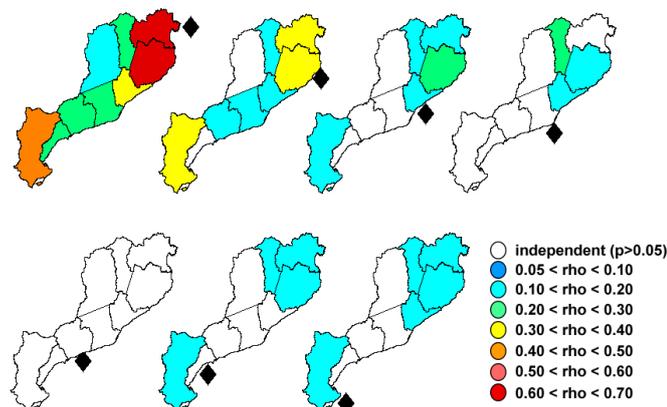
340

Figure 7. Correlation values (Spearman rho) between the Hs magnitude and P24h during compound events. Each map shows the correlation between the waves (Hs) at the area indicated by the diamond and rainfall in the other areas. White areas indicate that variables are statistically independent at a significance level of 0.05.

345   The results show that, in general, the correlation between the intensity of local wave storms and rainfall severities across the territory (measured as peak values of Hs and P24h during the event) decreases from north to south. The largest correlation values were obtained for the two areas in the north, where multivariate events dominated (Figure 6). The highest correlation (rho = ~0.65) was obtained for multivariate events in the northernmost area (Figure 7), suggesting a link between locally simultaneous wave storms and rainfall. The scale of the connection between the two analysed drivers extends southwards in

350   such a way that the correlation between the wave storm intensity in Area 1 with simultaneous rainfall episodes in the adjacent Area 2 is of the same order of magnitude. The correlation progressively decreases southward as we compare it with the rainfall recorded in the central basins, but, in all cases, the correlation is statistically different from zero. Notably, a value of rho > 0.4 is obtained in the southernmost sector, where the presence of multivariate events is higher than in the central basins.

355   When the intensity of wave storms recorded in Area 2 is correlated with rainfall across the territory during compound events (Figure 7), a similar behaviour with lower correlation values is observed. As we progressively move to the south, the correlation between the intensity of the locally recorded wave storms and P24h at any area consistently decreases to very low or statistically independent values. Thus, the central basins consistently have the lowest values of rho and independence from the waves.

360   **4.3. Synoptic conditions**

The classification of weather conditions during the 140 identified compound events resulted in three different synoptic types (Figure 8). Synoptic Type 1 conditions prevail during 42.1% of cases and are characterised by the presence of lower pressures northwest of the Iberian Peninsula over the Atlantic Sea and high pressures in the Central Mediterranean. The deep low in the north-western part of the Iberian Peninsula and the strong anticyclone over centre Europe favour a strong pressure gradient

365   and consequently induce intense winds from the south (Llasat, 1987). This type of situation usually creates a mesoscale structure when they impinge over the Pyrenees Range, known as an orographic dipole, with a mesoscale high over Catalonia that modifies the synoptic pressure field and creates an eastern component of the wind that favours the entrance of warm and wet air. At the same time, the mountain range triggers potential instability and develops convective systems and heavy rainfall (Trapero et al., 2013; Llasat et al., 2014b).

370

Synoptic Type 2 (18.6% of cases) is characterised by the presence of a depression in the south-eastern Iberian Peninsula and an anticyclone in the northwest, which creates a strong pressure gradient and N-NE winds. This kind of meteorological situation is more effective in generating sea storms than it is in generating floods. Synoptic Type 3 conditions (39.3% of cases) are similar to those of Type 2, with a deep low in the southern Iberian Peninsula and an anticyclone to the north-east. The main

375   difference is that this anticyclone is placed over the centre of Europe in this type; this pattern gives rise to a strong E-SE wind at low levels.
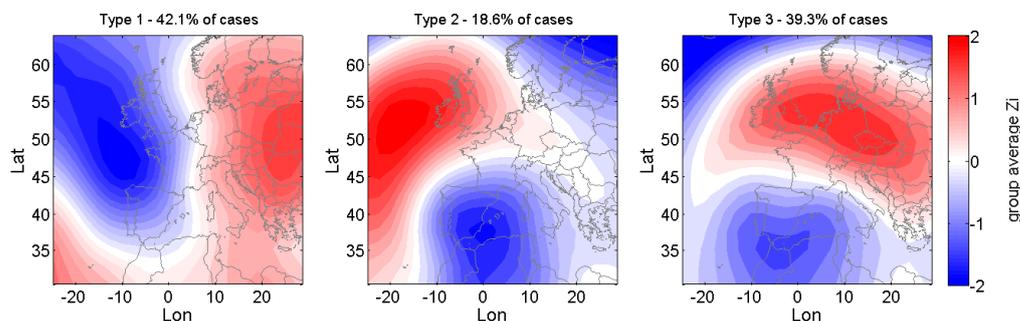
Figure 8. Synoptic types during the occurrence of compound extreme events along the Catalan coast based on the correlation between the 1000 hPa geopotential fields (coloured shades). The group average Zi represents the mean number of positive or negative
380   **standard deviations from the mean at each grid cell *i*.**

4.4. Compound event characteristics under each synoptic type

The BN was used to calculate the probability of occurrence of multivariate and spatially compounding (wave or rainfall) events in different areas given the different synoptic types (Figure 9); this allows the presence of each type of compound event to be assessed. The BN was also used to calculate the probability of exceedance of Hs and P24h at significant thresholds for each
385   combination of compound event type at the different areas along the coast to assess the intensity of each contributing component (Figure 10).
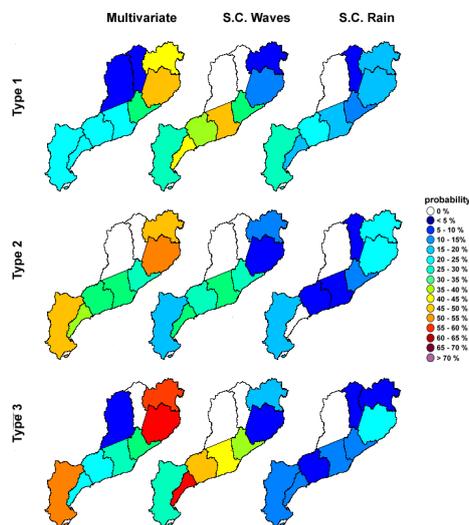
Figure 9. Spatial distribution of the probability of occurrence of the different types of compound events conditioned to each synoptic

390 **type. Probabilities are given per each area along the coast, and when adding the different types of events per area they do not**

necessarily reach 100% due to cases in which neither rainfall nor wave storms locally verify.
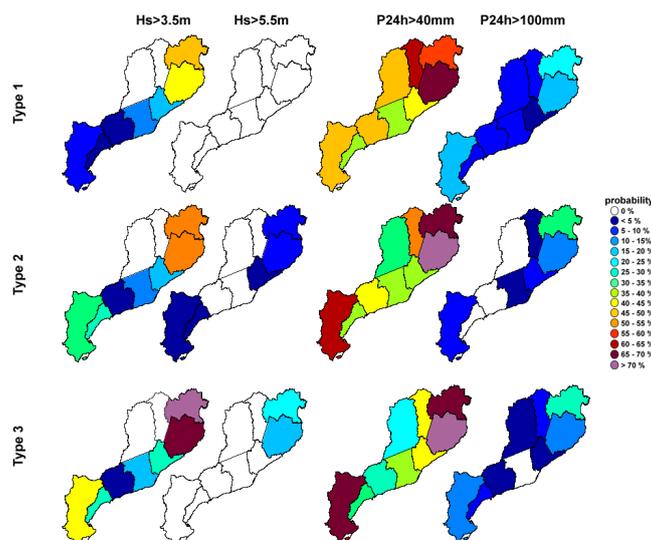
Figure 10. Spatial distribution of the probability of exceedance for different thresholds of Hs (3.5 m and 5.5 m) and P24h (40 and

395 **100 mm) conditioned to each synoptic type.**

Meteorological forcing under synoptic Type 1 is generally associated with the fewest compounding effects and the lowest severity of waves. They present the lowest probability of occurrence of multivariate events at the northern and southern extremes of the territory (where they are most likely to occur, Figure 6) when compared with the other types (Figure 9). In

400 areas along the central part of the coast, they induce spatially compounding events mostly dominated by local wave storms (Figure 9). Generated wave storms present smaller Hs values along the territory without inducing extreme storms (Hs > 5.5 m) (Figure 10). This type is also associated with the lowest probability of exceeding P24h > 40 mm in the northern and southern areas but had the highest probability of exceeding P24h > 40 mm and P24h > 100 mm in the central areas (3 to 6) and upper basins (2.b and 4.b). Notably, the probability of P24h > 100 mm is the highest across the territory, except for in Areas 1 and 4

405 (Figure 10).

Under synoptic Type 2, the probability of occurrence of multivariate events increases, especially in the northern and southern areas, while preserving a similar pattern as before for the central part of the coast where multivariate occurrences or spatially compounding waves are equally probable (Figure 9). The severity of coastal storms (Hs) increases, especially at the northern

410 and southern ends, where extreme storms (Hs > 5.5 m) have been recorded (Figure 10). The probability of rainfall episodes with P24h > 40 mm increases in the same areas with respect to Type 1, whereas the frequency of the most intense episodes (P24h > 100 mm) decreases, with the exception of Area 1 (Figure 10).

Conditions associated with synoptic Type 3 are similar to those under Type 2 but with the anticyclone placed over the centre

415 of Europe (Figure 8). Consequently, they present similar overall probabilities of occurrence of multivariate events along the coast, with Type 3 presenting an even larger probability of multivariate occurrence at the northern and southern extremes and a higher frequency of spatially compounding events dominated by local waves, especially in the central areas (Figure 9). In

terms of intensity, wave storms recorded under synoptic Type 3 present the highest probability of exceeding Hs > 3.5 m in all areas and the highest probability of extreme waves (Hs > 5.5 m), which is restricted to the two northernmost areas (Figure 10).

420 The spatial pattern of rainfall intensity for moderate events (P24h > 40 mm) is similar to that under Type 2 with intensification in Areas 1, 2, and 7, and severe episodes (P24h > 100 mm) are also similar to that under Type 2 with intensification in Areas 5, 6, and 7 (Figure 10).

5. Discussion

425 Differences in weather patterns result in particular event characteristics throughout the study area, which affects their induced impacts on individual basins. In order to show the potential consequences of these events and to put the analysis in the context of risk management, the impact of selected events recorded in the study area under the different synoptic types are illustrated with information gathered from after-event press coverage and the INUNGAMA database (Llasat et al., 2009, 2014a; Jiménez et al., 2012). Synoptic conditions during each analysed event are shown in Figures 11 and 12, with maps being extracted

430 following the criteria described in the methodological framework. Table 3 shows the maximum Hs and P24h recorded in each area along the coast during each event. Two representative events were chosen for Types 1 and 3, as they occur twice as frequently as Type 2 events do.

Between 6 and 8 November 1982, a compound event generated under a Type 1 synoptic situation (Figure 11) took place along

435 the Catalan coast. From a meteorological point of view, the event was dynamically forced, as it unfolded in the prefrontal and frontal zones of a strong Atlantic baroclinic storm, although the Pyrenees played a relevant role by triggering deep convection. The largest contribution of humidity was from the Atlantic (mainly tropical and subtropical regions but also from the north) with relevant additional input from the western Mediterranean (Insua-Costa et al., 2019). This was a very extensive episode of heavy rain affecting Portugal, Spain, Andorra, and France. Catastrophic flash floods and landslides occurred in the Upper

440 Llobregat Basin (Area 4.b) and Upper Ter Basin (Area 2.b) (Puigdefàbregas, 1983; Llasat, 1987), where nearly 342 mm and 556 mm were recorded in less than 24 h and 72 h, respectively. The Llobregat River (Areas 4.a and 4.b) recorded a peak flow of 1600 m^3/s near its mouth when its average discharge was 328 m^3/s.

The main peak rainfall and wave conditions recorded during the event along the Catalan coast are shown in Table 3. As can be

445 seen, although waves exceeded storm threshold conditions along the entire coast, their values were relatively low, with only the northernmost sector presenting severe storm conditions according to the Mendoza et al. (2011) classification. Due to this, coastal storm–induced damages were relatively low and were limited to some stretches at Costa Brava (Areas 1 and 2.a) where waves induced minor damage to some marina facilities and caused overtopping at some beach waterfronts. Some beaches in the Maresme region (Area 3) were also affected, with extensive erosion and overtopped promenades. On the other hand, the

450 rainfall-induced damage was extensive and very important, with 14 casualties and 1033 million € (adjusted for 2020) of private flood damages paid by the Insurance Compensation Consortium (the Spanish public re-insurance company, CCS) as a consequence of the floods in Catalonia (throughout the entire territory and not only in coastal areas). In summary, although this was a compound event, the most important and relevant damage was caused by rainfall-induced floods (Figure 12).

455 Another significant Type 1 event occurred in 2011, starting on 2 November and lasting until 7 November 2011 (Figure 11). It mainly affected Catalonia (Spain) and Liguria (Italy). In the first region, the maximum cumulative rainfall was 326 mm (close to Area 2.b, Table 3), while the maximum in 24 h was 203 mm (close to Area 4.b, Table 3). It produced a flood in the Muga River (Area 1) with a peak discharge of 378 m^3/s near the mouth (on 1 November the flow was 0.7 m^3/s) (Llasat et al., 2014). Between 2 and 8 November, the CCS paid 2.1 million € (adjusted for 2020) for damages produced by the sea storm and 458.8

460 million € (adjusted for 2020) for damages produced by floods in insured assets. Meteorological features showed the presence

of a trough at 500 hPa associated with a synoptic frontal wave that evolved into a mesoscale depression along the Catalan coast on 6 November. This situation favoured the entrance of very warm and wet air from the south-east over Catalonia and humidity advection from the Atlantic.

465 Notably, both events have the same characteristics we obtained with the results herein, indicating events with more contribution to the damage from the rainfall driver, with low reporting of the combined effects that may verify locally and moderate-to-high severity of the impacts.
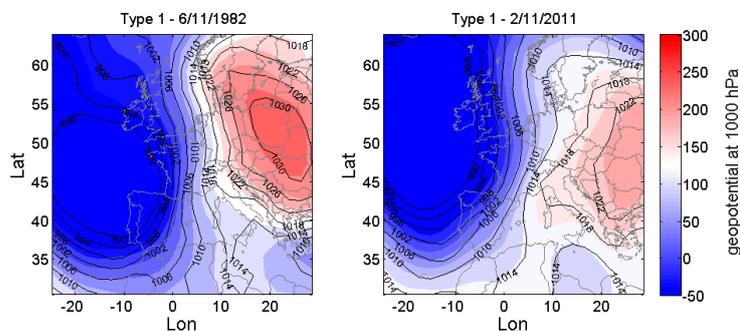
470 **Figure 11. Maps of the 1000 hPa geopotential fields (shades) and MSLPs (lines) of Type 1 events extracted at the time closest to the start of the coastal storm.**

An historical compound event generated under Type 2 conditions in the area occurred in November 2001 (Figure 12), when a thermal low over the African plateau interacted with an upper-level trough and developed a strong cyclone that moved toward

475 the Mediterranean Sea over Algiers following a northward trajectory, creating torrential rainfalls and floods in Algiers (more than 700 deaths). When the cyclone reached the sea, the low reached its mature state (Fita et al., 2006; Genovés and Jansà, 2002). The depression was observed at all atmospheric levels, and there was also a zone of high pressure that was located to the north-west of the Peninsula with a pressure higher than 1035 hPa that contributed to the strong wind and pressure gradients. The deep low continued its trajectory to the NE and affected Catalonia, giving rise to a windstorm with a recorded maximum

480 wind speed of 170 km/h (Port-Bou, Area 1). In contrast to the previously described Type 1 situation, this event was characterised by very high Hs values along the entire coast (Table 3), exceeding the threshold for severe storms according the Mendoza et al. (2011) storm classification in nearly all areas (except Area 5) and for extreme storms in the northernmost areas (1 and 2.a). Thus, compounding conditions were wave-dominated, with the rainfall being moderate (although exceeding the 40 mm threshold for P24h) except in the northernmost Area 1, where the P24h was higher than 100 mm. In addition, snowfall

485 in the northern part of the region and severe weather (a tornado in Montgat, Area 3, and hailstorms in Tarragona N and S, Areas 5 and 6) were also observed. Although many civil protection interventions due to floods and wind action occurred mostly in the central part of the study area, most of the incurred damage was due to coastal (wave) storm-induced hazards. Thus, the entire coastal zone was severely affected from south to north as the storm propagated along the coast (Figure 13). In the southernmost part (Area 7), the Ebro delta plain was extensively flooded, while the beaches were severely eroded. This resulted

490 in significant damage to rice fields and existing infrastructure. Along the entire coast, many ports and marinas were significantly overtopped, with the breakwater of the Port of Barcelona being damaged. In some stretches, such as Barcelona (Area 4.a) and some parts of Maresme (Area 3), many beaches were fully eroded, with their promenades being directly exposed to wave action; the coastal railway along Maresme was also impacted. In the northernmost part of the study site (Areas 1 and 2.a), coastal flooding occurred in several municipalities due to massive overtopping of beaches and promenades. In summary,

495 although this was a compound event, the most important and relevant damages were caused by coastal (wave) storm-induced
hazards (Figure 12).
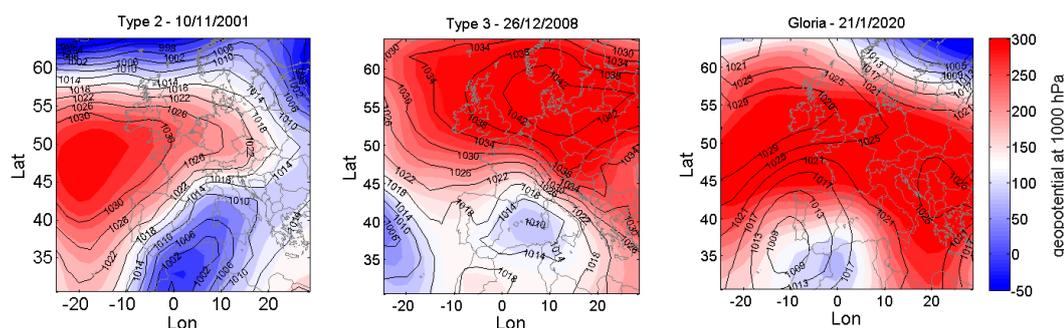
Figure 12. Maps of the 1000 hPa geopotential fields (shades) and MSLPs (lines) of Type 2 and Type 3 events extracted at the time
500 **closest to the start of the coastal storm.**

On 26 and 27 December 2008 (Type 3, Figure 12), a very intense coastal storm affected the Catalan coast and was accompanied
by strong winds, snow, and rain. The surface synoptic situation by 26 December was characterised by a pronounced anticyclone
in northern Europe extending from Ireland to Russia, centred in Denmark, and a low-pressure area with two clear centres over
505 Catalonia and Valencia and another located over the Azores. Along the Catalan coast, there was strong wet advection from the
south-east due to the strong low–high dipole. This situation caused a very high pressure gradient that produced strong advection
from the east and south-east of Catalonia. As a result, very high waves and rainfall were recorded along the study area, with
the highest values being reached in the northern half of the coast (Areas 1, 2.a, 3, and 4.a). In addition to tangible damage, four
fatalities occurred during the episode, three of which were associated with wave action and the fourth occurring from a flood
510 in the Muga River (Area 1 and Table 3). Extreme wave impacts along the coastline induced significant damage, with extensive
sediment losses in the beaches, promenades overtopped, and damage to infrastructure (Figure 13). This occurred especially in
the northern part of the coast (Areas 1 and 2.a) where waves reached values typical of extreme storms according to the Mendoza
et al. (2011) classification. This was one of the most important recorded coastal storms, with observed impacts also on
nearshore ecosystems (e.g. Sánchez-Vidal et al., 2012). On land, the strong wind uprooted a large number of trees and cut off
515 the electricity and telephone lines. The Fabra observatory in the city of Barcelona recorded a maximum wind gust of
approximately 85 km/h. During the event, notable snowfall at low altitudes, some landslides, and a tornado in Platja d'Aro
(Area 2.a) were produced. Many roads and train lines were cut off due to heavy snowfall and flooding of the tracks near the
sea. The Ministry of the Environment allocated an equivalent of 21.6 million € (adjusted for 2020) to different municipalities
on the Catalan coast to carry out emergency work with the aim of repairing the damage caused by the waves on beaches and
520 coastal infrastructure. The government granted aid packages to several municipalities and fishermen for more than 0.72 million
€ (adjusted for 2020).

Recently, the severe storm Gloria took place in the Catalan Sea in January 2020 (Figure 12) with record-breaking events
occurring in all areas for both wave heights and rainfall (Table 3). It started as a small superficial depression (about 600 km in
525 diameter) located in the central part of the North Atlantic Ocean, which was increasing in height while moving eastward. By
18 January, the storm had nearly doubled in size, while a high-pressure region was being reinforced further south. On 19 and
20 January, the high-pressure anticyclone zone moved to the north of the Gloria storm, leaving the latter over the south of the
Iberian Peninsula. Between 20 and 23 January, both areas were well defined in the form of a dipole creating a strong pressure

gradient that gave rise to very intense winds while favouring the entry of maritime air over the study area (Berdalet et al.,
2020). The synoptic pattern (on 20 January +00 UTC, closest to the coastal storm start time) corresponded to a Type 3 synoptic
event. Wave heights recorded during the peak of the storm along the Catalan coast reached record maximum values, and they
were accompanied by the presence of a moderate storm surge, reaching values of ~0.5 m in the southernmost area (Amores et
al., 2020; Jiménez, 2020). Wave impacts produced significant erosion at the beaches, with massive overtopping and flooding
of low-lying areas such as the Ebro delta, waterfronts, and marinas as well as structural damage in some coastal groins and
port breakwaters (Jiménez, 2020). The extreme coastal storm was accompanied by very intense rainfall and thunderstorms
throughout the territory, reaching record values from the last seven decades, which significantly contributed to flooding along
some coastal plains, occasional cut offs and damage to roads and railways. The Department of Interior of the Government of
Catalonia responsible for civil protection services activated three emergency plans for risk management: INUNCAT (flash
floods, river floods, and coastal floods), NEUCAT (snowfalls, significant above 600 m), and VENTCAT (wind, extreme
gusts lasting about 48 h, with a maximum of 144 km/h). These hazards caused four casualties (and 10 more in the Balearic
Islands and Valencia) and extensive damage throughout the territory (Figure 13), with a preliminary evaluation of payments
to be covered by the Spanish public re-insurance company (CCS) rising up to about 51 million €. Inversions to rebuild port
infrastructures affected by the storm are estimated to be about 17.4 million €; about 6 million € were budgeted by MITECO to
repair damage in the public coastal domain, and damage due to floods in the river margins and flood plains was estimated at
42 million € by the Catalan Water Agency (ACA).

Table 3. Values of the maximum Hs (m) and P24h (mm) for each selected event (Figures 10 and 11) along the study area extracted
from the analysis dataset. Data on Gloria (outside the dataset) was extracted from the SIMAR wave database (Puertos del Estado)
and XEMA rain gauge system (SMC). Note that the Hs values given for Gloria do not belong to the same database as the other
storms do; consequently, their values are not absolutely equivalent.

	Type 1				Type 2		Type 3			
	06/11/1982		02/11/2011		10/11/2001		26/12/2008		21/01/2020 (Gloria)	
	Hs (m)	P24h (mm)	Hs (m)	P24h (mm)	Hs (m)	P24h (mm)	Hs (m)	P24h (mm)	Hs (m)	P24h (mm)
Area 1	**5.4**	78	-	93	**7.9**	**107**	8.0	203	7.2	**101**
Area 2.a	4.6	98	-	46	**8.1**	81	**7.8**	120	6.1	204
Area 2.b		**196**		83		57		43		148
Area 3	4.3	**116**	-	56	**6.0**	-	5.4	60	6.0	115
Area 4.a	3.9	69	2.3	56	5.3	49	4.3	52	6.6	136
Area 4.b				**133**		59		-		131
Area 5	3.4	50	2.4	82	4.0	48	2.8	47	5.4	**154**
Area 6	3.1	-	2.4	-	**5.5**	50	3.8	-	**6.3**	126
Area 7	3.3	-	2.5	-	**5.6**	46	3.9	41	**7.6**	209

Notably, in agreement with the obtained results, both Type 2 and 3 extreme events (Figure 12) are more severe than Type 1 in
terms of coastal storms. Heavy rainfall produced local floods or dangerous discharges in ephemeral rivers in both Type 2 and
Type 3 events. Nonetheless, Type 3 events are potentially the most compounding and intense, with Gloria 2020 being a perfect
example of possible extreme impacts. The intensity and persistence of Gloria 2020 was unique, and looking at weather maps
of the event (Figure 12), it clearly has unique characteristics in its MSLP pattern that contrasts with the 1000 hPa geopotential
field compared to other events. Notably, the MSLP pattern resembles that of a synoptic Type 2 event, indicating transitions
between weather types during the duration of the events. This suggests that the role of the transitions in the characterisation of
compound events should be further studied.

Figure 13. Headlines in a local newspaper (La Vanguardia) after the impact of selected events (Figures 11 and 12). From top left to bottom right: (9/11/1982) "8 dead caused by floods in Catalonia" / "Segre and Llobregat basins, the most affected by the event"; (12/11/2001) "The storm hits the Catalan coast" / "Barcelona loses its beaches"; (28/12/2008) "The storm shakes the Catalan coast" / "The most intense rains" / "Like a wreck"; (16/11/2011) "The downpour punishes the Catalan coast" / " Flooding disrupts train and underground networks in Tarragona and Barcelona" / "Floods in Salou for the third time in a month" / "65 children evacuated from poorly-built schools"; (23/01/2020) "Gloria leaves a pathway of destruction and losses" / "The storm causes 10 dead (one in Palamós), 4 missing and all alarms triggered at the Ter basin" / "Final countdown at the Ebro Delta".

6. Conclusions

570 From the obtained results, the north-western Mediterranean coast represented by the Catalan littoral zone can be characterised as an area with a relatively high probability of experiencing compound extreme events (3.4 events per year) as defined in terms of heavy rainfall (P24h) and wave storms (Hs). The most frequently found type along the territory is the spatially compound event, which is mostly dominated by waves, whereas the influence of intense rainfall has a smaller spatial scale. However, even for the relatively small scale of the area (about 600 km of coastline), there is a significant variation in event characteristics

575 along the territory, which may have important implications for risk management. Thus, the two northernmost sectors (Girona N and Lower Ter–Tordera) are the most likely to suffer from multivariate compound events, in such a way that they are the only geographical areas in which their frequency of occurrence exceeds the other type. These areas also present the highest correlation in the intensity of both hazards (P24h and Hs). The other area in which multivariate events exceed the average frequency along the territory (although with a frequency smaller than spatially compound events) is the southernmost area (the

580 lower Ebro and delta, Area 7).

This pattern is verified under all synoptic situations, although with some particularities that are related to dominant weather conditions at the start of the compounding coastal storm. Thus, events generated under Type 1 conditions are dominated more by extreme rainfall because wave storms do not usually reach significantly high values, especially along the central part of the

585 coast. In contrast, compound events generated under Types 2 and 3 are more likely to be characterised by the presence of extreme coastal storms, especially in the north, where they might also be accompanied by extreme rainfall (P24h > 100 mm). Type 2 events occur half as frequently as Types 1 and 3 and are mainly associated with the occurrence of extreme waves (Hs > 5.5 m) at the northern and southern ends of the region. Under these synoptic situations, labelled as Mediterranean cyclones, the most extreme coastal storms have been recorded on the Catalan coast (Mendoza et al., 2011). Nonetheless, Type 3 events

590 can be as severe as Type 2 events in terms of waves, with higher probabilities of compounding simultaneous extreme rainfall.

Compound event characteristics under each dominant weather type in terms of the spatial distribution and intensity were characterised using a BN. With the exception of the two northernmost basins where multivariate events are dominant, the dominant typology is the spatially compound event (wave-dominated). This means that the extension of the affected area is

595 usually larger for waves than for flash floods. In spite of this, the damage associated with heavy rainfall is usually much larger than that due to wave action.

The selected historical compound events are good examples of their potential consequences in an economically developed NW Mediterranean coastal zone. Even at a relatively small regional scale, they have an uneven spatial distribution in terms of the

600 dominant typology, hazard severity (rain and waves), and the correlation between them. The dominant synoptic conditions under which these events are generated have been clearly identified, with each inducing different types of events.

Author contributions

605

JAJ and MCL conceived the study. MS prepared the methodological framework and analysed the data, with all authors discussing results and implications. MS and TR were responsible for data pre-processing and curation. MS prepared the manuscript with contributions of all authors. JAJ and MCL were responsible for funding acquisition and supervision.

610 **Acknowledgements**

This work has been done in the framework of the M-CostAdapt (CTM2017-83655-C2-1&2-R) research project, funded by the Spanish Ministry of Economy and Competitiveness (MINECO/AEI/FEDER, UE). The authors express their gratitude to IH-Cantabria for supplying wave data, and AEMET and SMC for supplying rain data. Our thanks to Montserrat Llasat-Botija for her contribution in the identification of the compound events as well as for all the information about the impacts

615 **References**

Alfieri, L., Burek, P., Feyen, L., Forzieri, G., 2015. Global warming increases the frequency of river floods in Europe. Hydrol. Earth Syst. Sci. 19, 2247–2260. https://doi.org/10.5194/hess-19-2247-2015

Amores, A., Marcos, M., Carrió, D. S., & Gómez-Pujol, L. Coastal impacts of Storm Gloria (January 2020) over the north-western Mediterranean. Natural Hazards and Earth System Sciences, 20(7), 1955-1968. 2020.

620 Ballesteros, C., Jiménez, J.A., and Viavattene, C.: A multi-component flood risk assessment in the Maresme coast (NW Mediterranean). Natural Hazards 90, 265-292, doi: 10.1007/s11069-017-3042-9, 2018.

Barbería, J. Amaro, M. Aran, and M. C. Llasat. The role of different factors related to social impact of heavy rain events: considerations about the intensity thresholds in densely populated areas. Nat. Hazards Earth Syst. Sci., 14, 1843–1852, 2014

Barnolas, M. and M.C. Llasat: A flood geodatabase and its climatological applications: the case of Catalonia for the last 625 century. Natural Hazards and Earth System Sciences, 7, 271-281, 2007.

Berghuijs, W. R., Harrigan, S., Molnar, P., Slater, L. J. & Kirchner, J. W. The relative importance of different flood-generating mechanisms across Europe. Wat. Resour. Res.55, 4582–4593, 2019.

Beuzen, T., Splinter, K.D., Marshall, L.A., Turner, I.L., Harley, M.D., Palmsten, M.L. Bayesian Networks in coastal engineering: Distinguishing descriptive and predictive applications. Coast. Eng. 135, 16–30. 630 https://doi.org/10.1016/j.coastaleng.2018.01.005. 2018.

Bevacqua, E., Maraun, D., Vousdoukas, M. I., Voukouvalas, E., Vrac, M., Mentaschi, L., and Widmann, M.: Higher probability of compound flooding from precipitation and storm surge in Europe under anthropogenic climate change. Science advances, 5(9), eaaw5531, 9, eaaw5531, doi: 10.1126/sciadv.aaw5531, 2019.

Blöschl, G., A. Kiss, A. Viglione, M. M. Barriendos, O. et al, 2020. Current flood-rich period is exceptional compared to the 635 past 500 years in Europe. Nature 583, 560-566. https://doi.org/10.1038/s41586-020-2478-3.

Bolaños, R., Jordá, G., Cateura, J., Lopez, J., Puigdefabregas, J., Gómez, J., and Espino, M.: The XIOM: 20 years of a regional coastal observatory in the Spanish Catalan coast. Journal of Marine Systems 77, 237-260, doi: 10.1016/j.jmarsys.2007.12.018, 2009.

Bosom, E., Jiménez, J.A. Probabilistic Coastal vulnerability assessment to storms at regional scale. Application to Catalan 640 beaches (NW Mediterranean). Natural Hazards & Earth System Sciences 11, 475-484. https://doi.org/10.5194/nhess-11-475-2011, 2011

Camus, P., Mendez, F.J., Medina, R., Tomas, A., and Izaguirre, C.: High resolution downscaled ocean waves (DOW) reanalysis in coastal areas. Coast. Eng. 72, 56–68, doi: 10.1016/j.coastaleng.2012.09.002, 2013.

Casas-Prat, M., and Sierra-Pedrico, J.P.: Trend analysis of wave storminess: wave direction and its impact on harbour agitation. 645 Natural Hazards and Earth System Sciences 10, 2327-2340, doi: 10.5194/nhess-10-2327-2010, 2010.

Cortès, M., M. Turco, M. Llasat-Botija, M. C. Llasat. The relationship between precipitation and insurance data for floods in a Mediterranean region (Northeast Spain). Nat. Hazards Earth Syst. Sci., 18, 857–868, doi.org/10.5194/nhess-18-857-2018, 2018.

Cramer, W., Guiot, J., Fader, M., Garrabou, J. et al.: Climate change and interconnected risks to sustainable development in 650 the Mediterranean. Nature Climate Change, 8(11), 972-980, 2018.

Fita, L., R. Romero, and C. Ramis: Intercomparison of intense cyclogenesis events over the Mediterranean basin based on baroclinic and diabatic influences.Adv. Geosciences, 7, 333-342, 2006.

Garnier, E., Ciavola, P., Spencer, T., Ferreira, O., Armaroli, C., McIvor, A.: Historical analysis of storm events: case studies in France, England, Portugal and Italy. Coastal Engineering, 134, 10-23, 2018.

Gaume, E., M. Borga, M.C. Llasat, S. Maouche, M. Lang, M. Diakakis. Mediterranean extreme floods and flash floods. Into Hydro-meteorological extremes, chapter 3, The Mediterranean Region under Climate Change. A Scientific Update (coordinated byAllEnvi).133-144. IRD Éditions Institut de Recherche pour le Développement, Marseille, 2016, ISBN : 978-2-7099-2219-7, 2016.

Genest, C., Favre, A-C. Everything you always wanted to know about copula modeling but were afraid to ask. Journal of Hydrologic Engineering 12(4), 347-368, 2007.

Genovés, A., Jansà, A., Diabatic processes contribution to the november 2001 storm, Mediterranean Storms, Proceedings of the 4th EGS Plinius Conference, Mallorca, Spain, 2002.

Gilabert, J. and Llasat, M.C. Circulation weather types associated with extreme flood events in Northwestern Mediterranean. Int. J. Climatol, 38: 1864-1876. doi:10.1002/joc.5301, 2017.

Gutierrez, B. T., Plant, N. G. and Thieler, E. R. A Bayesian network to predict coastal vulnerability to sea level rise, J. Geophys. Res. Earth Surf., 116(2), 1–15, doi:10.1029/2010JF001891, 2011.

Hall, J., B. Arheimer, M. Borga, R. Brázdil, P. Claps, A. Kiss, T. R. Kjeldsen, J. Kriaučiūnienė, Z. W. Kundzewicz, M. Lang, M. C. Llasat, N. Macdonald, N. McIntyre, L. Mediero, B. Merz, R. Merz, P. Molnar, A. Montanari, C. Neuhold, J. Parajka, R. A. P. Perdigão, L. Plavcová1, M. Rogger, J. L. Salinas, E. Sauquet, C. Schär, J. Szolgay, A. Viglione and G. Blöschl: Understanding Flood Regime Changes in Europe: A state of the art assessment. Hydrol. Earth Syst. Sci., 18, 2735-2772, doi:10.5194/hess-18-2735-2014, 2014.

Hallegatte, S., Green, C., Nicholls, R. J., and Corfee-Morlot, J.: Future flood losses in major coastal cities. Nature climate change, 3(9), 802-806, doi: 10.1038/nclimate1979, 2013.

Hao, Z., Singh, V.P. and Hao, F. Compound extremes in hydroclimatology: a review. Water, 10(6), p.718, 2018.

Hendry, A., Haigh, I., Nicholls, R., Winter, H., Neal, R., Wahl, T., Joly-Laugel, A., and Darby, S.: Assessing the characteristics and drivers of compound flooding events around the UK coast. Hydrol. Earth Syst. Sci., 23, 3117-3139 , doi: 10.5194/hess-23-3117-2019, 2019.

Insua-Costa, D., G. Miguez-Macho y M.C. Llasat. The role of remote and local moisture sources in the two famous 1982 Western Mediterranean torrential rainfall episodes. Hydrol. Earth Syst. Sci., 23, 3885–3900, https://doi.org/10.5194/hess-23-3885-2019, 2019.

IPCC. Summary for Policymakers, in Climate Change 2014: Impacts, Adaptation, and Vulnerability. Part A: Global and Sectoral Aspects. Contribution of Working Group II to the Fifth Assessment Report of the Intergovernmental Panel on Climate Change, eds. Field CB, Barros VR, Dokken DJ, Mach KJ, Mastrandrea MD et al. (Cambridge, United Kingdom and New York, NY, USA: Cambridge University Press), 1–32, 2014.

IPCC. Special Report on Managing the Risks of Extreme Events and Disasters to Advance Climate Change Adaptation. Field, C.B., V. Barros, T.F. Stocker, D. Qin, D.J. Dokken, K.L. Ebi, M.D. Mastrandrea, K.J. Mach, G.-K. Plattner, S.K. Allen, M. Tignor, and P.M. Midgley (Eds). Cambridge Univ. Press, 2012.

Jansà, A., P. Alpert, P. Arbogast, A. Buzzi, B. Ivancan-Picek, V. Kotroni, M. C. Llasat, C. Ramis, E. Richard, R. Romero, and A. Speranza (2014). MEDEX: a general overview. Nat. Hazards Earth Syst. Sci., 14, 1965-198. doi:10.5194/nhess-14-1965-2014.

Jensen, F. V. An introduction to Bayesian networks, UCL Press, London, UK, 1996.

Jiménez, J.A. Dinàmica litoral, efectes dels temporals i comportament de les platges. In M. Canals and J. Miranda (Eds.): Sobre el temporal Gloria (19-23.01.20), els seus efectes sobre el país i el que se'n deriva. Report de Resposta Ràpida (R3); Institut d'Estudis Catalans, Col·lecció Informes, Informe de la Secció de Ciències i Tecnologia, Barcelona (Spain), p. 55-7, 2020.

Jiménez, J.A., Sancho, A., Bosom, E., Valdemoro, H.I., and Guillén, J.: Storm-induced damages along the Catalan coast (NW Mediterranean) during the period 1958-2008. Geomorphology, 143-144, 24-33, doi: 10.1016/j.geomorph.2011.07.034, 2012.

Jiménez, J.A., Valdemoro, H.I.: Shoreline evolution and its management implications in beaches along the Catalan coast. In: Morales, J.A. (ed), The Spanish Coastal Systems Dynamic Processes, Sediments and Management, Springer, 745-764, 2019.

Kalnay et al., The NCEP/NCAR 40-year reanalysis project, Bull. Amer. Meteor. Soc., 77, 437-470, 1996.

Kanamitsu et al, NCEP-DOE AMIP-II Reanalysis (R-2). Bull. Amer. Meteor. Soc., 83, 1631-1643, 2002.

Kemp, M. U., Emiel van Loon, E., Shamoun-Baranes, J., Bouten, W. RNCEP: global weather and climate data at your fingertips. Methods in Ecology and Evolution (3), 65-70., DOI: 10.1111/j.2041-210X.2011.00138.x, 2012

705   Kron, W.: Coasts: the high-risk areas of the world. Nat. Hazards, 66, 1363-1382, doi: 10.1007/s11069-012-0215-4, 2013.

Llasat, M.C. y M. Puigcerver, 1992. Pluies extremes en Catalogne: influence orographique et caractéristiques synoptiques. Hydrologie Continentale, 2, 99-115. (Ed. Orstom). ISSN: 0246-1528. Paris, Francia. 1992.

Llasat, M.C., 1987, 'Episodios de lluvias copiosas en Cataluña: génesis, evolución y factores coadyu-vantes', Tesis Doctoral, Publicacions de la Universitat de Bar-ce-lona, 2, 424-448 pp

710   Llasat, M.C., Llasat-Botija, M., and López, L.: A press database on natural risks and its application in the study of floods in Northeastern Spain, Nat. Hazards Earth Syst. Sci., 9, 2049–2061, doi:10.5194/nhess-9-2049-2009, 2009.

Llasat, M.C., O. Caumont, I. Flores, L. Garrote, J. Gilabert, M. Llasat-Botija, R. Marcos, O. Nuissier, E. Richard, T.Rigo. THE 6 NOVEMBER 2011 FLOOD EVENT IN CATALONIA: ANALYSIS USING THE DRIHM INFRASTRUCTURE. Proceedings of the Mediterranean Meeting on "Monitoring, modelling and early warning of a extreme events triggered by heavy rainfalls". MED-FRIEND project University of Calabria, Cosenza (Italy), June 26-28, 2014a.

715

Llasat, M.C., R. Marcos, M. Llasat-Botija, J. Gilabert, M. Turco, P. Quintana. Flash flood evolution in North-Western Mediterranean. Atmospheric Research 149, 230–243, 2014b.

Llasat, M.C., R. Marcos, M. Turco, J. Gilabert, M. Llasat-Botija. Trends in flash flood events versus convective precipitation in the mediterranean region: the case of catalonia. Journal of Hydrology, 541, 24-37, 2016.

720   Mendoza, E.T., and Jiménez, J.A. Regional vulnerability analysis of Catalan beaches to storms. Proc. ICE- Marit. Eng., 162, 127-135, doi: 10.1680/maen.2009.162.3.127, 2009.

Mendoza, E.T., Jiménez, J.A., and Mateo, J.: A coastal storms intensity scale for the Catalan sea (NW Mediterranean), Nat. Hazards Earth Syst. Sci., 11, 2453-2462, doi: 10.5194/nhess-11-2453-2011, 2011.

Michaelides, S., T. Karacostas, J. L. Sánchez, A. Retalis, I. Pytharoulis, V. Homar, R. Romero, P. Zanis, C. Giannakopoulos,

725   J. Bühl, A. Ansmann, A. Merino, P. Melcón, K. Lagouvardos, V. Kotroni, A. Bruggeman, J. I. López-Moreno, C. Berthet, E.

Katragkou, F. Tymvios, R. E. Mamouri, and A. Nisantzi: Reviews and perspectives of high impact atmospheric process in the

Mediterranean. Atmos. Res., 208, 4-44, 2018.

Moftakhari, H.R., Salvadori, G., AghaKouchak, A., Sanders, B.F. and Matthew, R.A., 2017. Compounding effects of sea level rise and fluvial flooding. Proceedings of the National Academy of Sciences, 114(37), pp.9785-9790.

730   Paprotny, D., Vousdoukas, M.I., Morales-Nápoles, O., Jonkman, S.N. and Feyen, L. Compound flood potential in Europe. Hydrology and Earth System Sciences Discussions, pp.1-34, 2018.

Pearl, J. Probabilistic reasoning in intelligent systems: networks of plausible inference, Morgan Kaufmann, San Francisco, California, USA. 1988.

Plant, N. G., Robert Thieler, E., & Passeri, D. L. Coupling centennial-scale shoreline change to sea-level rise and coastal
735   morphology in the Gulf of Mexico using a Bayesian network. Earth's Future, 4(5), 143-158, 2016.

Puigdefàbregas.'Efectes geomorfològics dels aiguats del novembre de 1982', Publicacions del Servei Geològic de Catalunya. Departament de Política Territorial i Obres Públiques, 236 pp. 1983.

Ramis C, Homar V, Amengual A, Romero R, Alonso S. Daily precipitation records over mainland Spain and the Balearic Islands. Natural Hazards Earth System Science 13: 2483-2491. doi: 10.5194/nhess-13-2483-2013., 2013

740   Raymond, C., Horton, R.M., Zscheischler, J. et al.: Understanding and managing connected extreme events, Nat. Clim. Chang. 10, 611–621, doi: 10.1038/s41558-020-0790-4, 2020.

Reguero, B.G., Menéndez, M., Méndez, F.J., Mínguez, R., and Losada, I.J.: A Global Ocean wave (GOW) calibrated reanalysis from 1948 onwards, Coast Eng, 65, 38-55, doi: 10.1016/j.coastaleng.2012.03.003, 2012.

Sanuy M, Jiménez JA, Ortego MI, Toimil A. Differences in assigning probabilities to coastal inundation hazard estimators:
745   Event versus response approaches. J Flood Risk Management, e12557. https://doi.org/10.1111/jfr3.12557, 2019

Trapero, L., J. Bech, F. Duffourg, P. Esteban and J. Lorente. Mesoscale numerical analysis of the historical November 1982 heavy precipitation event over Andorra (Eastern Pyrenees), Nat. Hazards Earth Syst. Sci., 13, 2969-2990, 2013

Van Dongeren, A., Ciavola, P., Martinez, G., Viavattene, C., Bogaard, T., Ferreira, O., Higgins, R., McCall, R. Introduction to RISC-KIT: Resilience-increasing strategies for coasts. Coastal Engineering 134, 2-9, 750 doi.org/10.1016/j.coastaleng.2017.10.007, 2018

Vinet, F., V. Bigot, O. Petrucci, K. Papagiannaki, M.C. Llasat, V. Kotroni, L. Boissier, L. Aceto, M. Grimalt, M. Llasat-Botija, A.A. Pasqua, J. Rossello, Ö.Kılıç, A. Kahraman, and Y. Tramblay. Mapping Flood-Related Mortality in the Mediterranean Basin. Results from the MEFF v2.0 DB. Water 2019, 11, 2196; doi:10.3390/w11102196, 2019

Wahl, T., Jain, S., Bender, J., Meyers, S. D., and Luther, M.E.: Increasing risk of compound flooding from storm surge and 755 rainfall for major US cities, Nat. Clim. Change, 5, 1093–1097, doi: 10.1038/nclimate2736, 2015.

Ward, P.J., Couasnon, A., Eilander, D., Haigh, I.D., Hendry, A., Muis, S., Veldkamp, T.I., Winsemius, H.C. and Wahl, T. Dependence between high sea-level and high river discharge increases flood hazard in global deltas and estuaries. Environmental Research Letters, 13(8), p.084012, 2018.

Wu, W., McInnes, K., O'grady, J., Hoeke, R., Leonard, M. and Westra, S. Mapping dependence between extreme rainfall and 760 storm surge. Journal of Geophysical Research: Oceans, 123(4), pp.2461-2474, 2018.

Yarnal, B. Synoptic climatology in environmental analysis. London, UK: Belhaven Press. 1993.

Zscheischler, J., Martius, O., Westra, S., et al.: A typology of compound weather and climate events, Nat. Rev. Earth Environ., 1, 333-347, doi: 10.1038/s43017-020-0060-z, 2020.